Nature. Author manuscript; available in PMC 2015 June 04.

Published in final edited form as:
Nature. 2014 December 4; 516(7529): 90–93. doi:10.1038/nature13889.

Inhibition of cell expansion by rapid ABP1-mediated auxin effect on microtubules

Xu Chen[1,2], **Laurie Grandont**[3], **Hongjiang Li**[1,2], **Robert Hauschild**[1], **Sébastien Paque**[3], **Anas Abuzeineh**[2], **Hana Rakusová**[1,2], **Eva Benkova**[1,2], **Catherine Perrot-Rechenmann**[3,*], and **Jiří Friml**[1,2,*]

[1]Institute of Science and Technology Austria (IST Austria), Am Campus 1, 3400 Klosterneuburg, Austria

[2]Department of Plant Systems Biology, VIB and Department of Plant Biotechnology and Genetics, Ghent University, B-9052 Gent, Belgium

[3]Institut des Sciences du Végétal, UPR2355 CNRS, Saclay Plant Sciences LabEx, 1 Avenue de la Terrasse, 91198 Gif sur Yvette, Cedex, France

Abstract

The prominent and evolutionary ancient effect of the plant hormone auxin is the regulation of cell expansion[1]. Cell expansion requires ordered cytoskeleton arrangement[2] but molecular mechanisms underlying its regulation by signaling molecules including auxin are unknown. Here we show in the model plant *Arabidopsis thaliana* that in elongating cells exogenous application of auxin or redistribution of endogenous auxin induces very rapid microtubule reorientation from transversal to longitudinal, coherent with the inhibition of cell expansion. This fast auxin effect requires Auxin Binding Protein1 (ABP1) and involves a contribution of downstream signaling components such as ROP6 GTPase, ROP-interactive protein RIC1 and microtubule severing protein Katanin. These components are required for rapid auxin and ABP1-mediated reorientation of microtubules to regulate cell elongation in roots and dark grown hypocotyls as well as asymmetric growth during gravitropic responses.

Auxin is crucial for diverse developmental processes and growth responses[3]. One of the major auxin effect is cell expansion[1], which relies on the coordinated activities of cellular processes involving cytoskeleton[2]. When cells elongate, cortical microtubules (MTs) are arranged perpendicular to the cell elongation's axis (transversal MTs), whereas a longitudinal alignment accompanies growth inhibition[2]. The dynamic nature of MTs

Correspondence and requests for materials should be addressed to J.F. and C. P.R. (jiri.friml@ist.ac.at, Catherine.Rechenmann@isv.cnrs-gif.fr).
*Co-corresponding authors

Author contributions

X.C., L.G., C.P.R., and J.F. conceived the study and designed experiments. X.C. carried out experiments in roots, and L.G. carried out experiments in hypocotyls. H.L., S.P. and A.A. assisted in microscopy and data generation. H. R. generated partial double mutants. R.H. did bioinformatics analysis. E.B. helped discussion of the data. X.C., L.G., C.P.R. and J.F. wrote the manuscript.

The authors declare no competing financial interests.

Europe PMC Funders Author Manuscripts

provides the flexibility to rearrange into different arrays[4], enabling growth changes downstream of different signals such as gravity[5] or light[6]. Many of these signaling pathways converge on auxin[7], therefore its action upstream of MTs translates different signals into growth responses[1]. Nonetheless, whether auxin acts directly on MTs arrangement and by which mechanism remain unclear.

MTs coalign approximately in perpendicular to the elongation axis in roots and dark grown hypocotyls[4]. The transition zone of primary root and the elongation zone of etiolated hypocotyl (Extended Data Fig. 1a) are controlled by auxin to determine their respective growth rates[7]. We visualized cortical MTs in transgenic lines expressing Microtubule-Associated Protein4 (MAP4-GFP)[8] or α-Tubulin6 (TUA6-RFP)[9] and classified cells based on prevalent MT arrangement into four groups (Fig. 1a). In root, MTs were mainly transversal and underwent visible realignment within 10 min after application of the synthetic auxin NAA, leading to partial longitudinal reorientation after 1 h (Fig. 1a). Comparable effects were observed irrespective of the MT reporter following treatment with the natural auxin IAA (Extended Data Fig. 1b-f). The same effects were observed in etiolated hypocotyls (Fig. 1b) although at a higher auxin concentration consistent with known auxin response maxima of aerial tissues at higher doses[10]. Reorientation of MTs is not always homogenous as revealed by the deviated angle of individual MTs. Transversal MTs (90±30°) decreased at the expense of increasingly oblique and longitudinal MTs (0-60°/120-180°) following auxin treatment (Extended Data Fig. 1c, f).

Treatment with the weak auxin analog[11] of 2-naphthaleneacetic acid (2-NAA) showed very weak effect on MT rearrangement whereas acidic pH led to massive disruption and random orientations of MTs (Extended Data Fig. 1g, h). Both treatments confirm the specificity of active auxins on MTs orientation.

In roots, gravistimulation induces asymmetric auxin redistribution with lower levels at the upper side (US) correlating with cell elongation and higher levels at the lower side (LS) with inhibition of cell expansion[12]. We assessed the effect of endogenous auxin redistribution on MTs arrangement by tracking trajectories of End Binding1b (EB1b) that preferentially accumulates at the growing plus ends of MTs[13]. After 90° root reorientation, transversal MTs were maintained in the US cells whereas at the LS, MT longitudinally reoriented within 10 min, preceding growth inhibition (Fig. 1c). Auxin distribution reported by the auxin response reporter DII:Venus[14] during gravitropism confirmed higher auxin response at the LS compared to the US (Extended Data Fig. 1i-k). Thus auxin application or endogenous auxin redistribution promotes longitudinal MTs orientation, correlating with auxin inhibiting cell elongation.

Next we addressed the mechanism by which auxin influences MTs orientation. The signaling pathway TIR1/AFB (Transport Inhibitor Response1/Auxin-Related F-BOX)-Aux/IAA nuclear-localized auxin co-receptors regulates gene transcription and mediates many plant developmental effects[3]. On the other hand, the ABP1 pathway regulates transcriptional[15] and non-transcriptional responses such as interdigitation of pavement cells[16] or clathrin-dependent endocytosis[17].

In root cells of *tir1-1afb1-1abf2-1afb3-1*[18], we observed normal transversal MTs, however they were less sensitive to auxin treatment (Extended Data Fig. 2a, b). Functional inactivation of ABP1 in the conditional SS12S and SS12K lines[19,20] resulted in MT orientation defects with increasing time of ABP1 inactivation (Extended Data Fig. 2c-f), whereas *abp1-5*, harboring a point mutation in the auxin binding pocket susceptible to impair auxin binding[16], did not show altered MTs arrangement (Fig. 2a). Nonetheless, in both cases a severe reduction of MT reorientation was observed in response to auxin (Fig. 2a). Short term ABP1 inactivation (8 h) in dark grown hypocotyls also impaired MT responsiveness to auxin without affecting the MT organization per se (Fig. 2b). This observation together with similar effect of *abp1-5* mutation confirms that the MT insensitivity to auxin does not result from pre-existing MTs alteration in these lines. Growth of ABP1-inactivated roots were previously reported to be auxin resistant[20], strengthening the correlation between auxin effect on MT orientation and inhibition of cell elongation.

We also explored whether ABP1 function is required for the MT rearrangement and differential growth response in root gravitropism. Following 90° root reorientation, ABP1-inactivated lines showed much weaker MT rearrangement at the LS compared to WT (Extended Data Fig. 3a); however, gravity-induced asymmetric auxin distribution (monitored by DII:Venus) was also less pronounced in ABP1-inactivation lines (Extended Data Fig. 3b-c compared with Extended Data Fig.1i-k). In line with these observations, ABP1-deficient lines showed defects in gravitropic response (Extended Data Fig. 3d).

Given the mutual impact of the TIR1 and ABP1 pathways[15], it is difficult to distinguish between direct and indirect effects, but because short-term ABP1 inactivation strongly impairs auxin—mediated MT reorientation favors ABP1 pathway as the primary mechanism. To gain further mechanistic insights into auxin effect on MT and transcriptional vs. fast, non-transcriptional responses, we studied kinetics of auxin effect on MT reorientations by following EB1b movement at 15 sec intervals, and its trajectories. NAA did not influence the speed of EB1b movement (Extended Data Fig. 4a, b) but gradually increased oblique and longitudinal EB1b tracks (0-60°/120-180°) after 75 sec (Fig. 3a, Supplementary Video 1, 2). To provide quantitative measures of MT rearrangements, we developed an image analysis tool that automatically assigned EB1b trajectories to be transversal (depicted as blue area) or longitudinal (red area) directions, which revealed changes in EB1b track orientations as soon as 30 sec after auxin treatment (Extended Data Fig. 4c). Both types of kinetic analysis revealed a very fast responsiveness of MTs to auxin making transcriptional regulation in this process unlikely. This is consistent with the lack of interference on auxin-induced MT rearrangement by blocking transcription with cordecypin (Extended Data Fig. 4d). Involvement of the ABP1-dependent response pathway is also supported by the inhibition of TIR1/AFB pathway with PEO-IAA (α-(phenylethyl-2-one)-IAA)[21] that did not prevent IAA effect on MT (Extended Data Fig.4e).

To further investigate the rapid ABP1-dependent effect on MTs, we introduced EB1b-GFP in ABP1-inactivated lines. Trajectories of EB1b following ABP1 inactivation showed more oblique and longitudinal MTs in comparison to WT (Fig. 3b, Extended Data Fig. 4f-i, Supplementary Video 3, 4). After NAA treatment, no consistent switch of EB1b trajectories to longitudinal directions but only few stochastic changes were observed (Supplementary

Video 5, 6, Fig. 3b, Extended Data Fig. 4f-i compared to WT in Fig. 3a, Extended Data Fig. 4c). By a complementary approach, we analyzed the effect of auxin on EB1b trajectories in inducible ABP1 gain-of-function lines (XVE>>ABP1-OE). Overexpression of ABP1-GFP in the presence of estradiol increased the overall amount of ABP1 (Extended Data Fig. 5a-c), leading to an enhanced MT reorientation in response to auxin (Extended Data Fig. 5d). In contrast, *abp1-5* exhibited delayed MT reorientation in response to auxin (Extended Data Fig. 5d). Overall these results strongly suggest that fast, non-transcriptional effect of auxin on MT reorientation is mediated primarily by ABP1-dependent signaling.

Next we addressed the downstream mechanism by which ABP1 mediates the auxin effect on MT arrangement. Although auxin induces calcium transients[22], the manipulation of exogenous calcium had very different effects on MT arrangements as compared to auxin (Extended Data Fig. 6). Next we tested the downstream components of ABP1 pathway: the ROP6 GTPase, its effector RIC1[16] and its downstream component MT severing protein KTN1[23,24]. We analyzed MTs in *rop6-1*, *ric1-1* and *ktn1* mutants. Compared to WT, roots of *rop6-1* and *ric1-1* showed almost normal transversal MTs but were much less auxin responsive (Fig. 4a, Extended Data Fig. 7a). Double mutants (SS12S *ric1-1*, SS12K *ric1-1*), with ABP1 inactivation, exhibited SS12K/S root phenotype[15] but *ric1-1* MT arrangement (Fig. 4a, Extended Data Fig. 7a-d), consistent with RIC1 reported action downstream of ABP1 in early responses[25]. *ktn1* mutant exhibited severe MTs phenotype with completely random MTs in root compromising further analysis. MTs were less disturbed in dark grown *ktn1* hypocotyl allowing investigating the response to auxin and genetic interaction with ABP1 (Extended Data Fig. 7e). Rapid auxin-induced reorientation of MTs was impaired in *ktn1* (Fig. 4b). Inactivation of ABP1 in *ktn1* (SS12K *ktn1*) resulted in a MT pattern similar to SS12K and confers insensitivity to auxin (Fig. 4b). These data suggest that KTN1 is required for MTs reorientation in response to auxin but that other MT associated components might be involved as well. The present data and the crucial roles of RIC1 and KTN1 in the control of microtubule architecture and crossover[6,24] support that auxin-dependent ABP1 signaling might act through Rho GTPases and RIC effectors on critical targets as KTN1 for guiding MT orientation.

Auxin effects on cell expansion are not mechanistically well understood but it is clear that sustainable growth control requires fast non-transcriptional auxin effects and regulation of transcription[3]. Here, we show that auxin signaling targets immediate changes in MT orientation. Auxin, by a non-transcriptional effect requiring ABP1 and downstream signaling, influences within minutes MT reorientations leading to change of MTs from transversal to longitudinal orientation to inhibit cell elongation. It is possible that branching of the ABP1 signaling for MT realignment occurs at the level of Rho GTPases, their RIC effectors and downstream target as KTN1. It remains unclear how this newly identified effect of ABP1 signaling on MTs is related to other actions of ABP1 pathway, such as inhibition of clathrin-mediated endocytosis, in particular given the differences in efficiencies of synthetic and natural auxins on both processes[26]. The relationship between MT and endocytosis in plants is still unclear but given the observations from animals that clathrin controls microtubule acetylation[27], auxin-mediated defect in clathrin organization might cause the mis-modification of MT and thus disturbs their crossover. On the other hand, Rho

GTPases acting downstream of ABP1 might influence clathrin and MT functions via distinct effectors. Our observations on the rapid regulation of MT arrangement by ABP1-mediated auxin signaling pathway provides insight into the long sought molecular mechanism by which a major plant hormone exerts its fast effect on plant cell growth.

METHODS SUMMARY

Material and growth conditions

Seeds were sown on 0.8% agar containing 1/2 Murashige and Skoog (MS) media without sucrose for root experiments and 1% agar containing 1/2 MS media without sucrose for hypocotyl experiments. For root analyses, seedlings were grown under 16h light/ 8h dark photoperiod and for hypocotyl analyses seedlings were grown in darkness at 22° for four days. Ethanol induction of conditional lines for ABP1[19] (named SS12S or SS12K) was performed by exposure of the seedlings to ethanol vapor for various times as indicated for the different assays. We routinely used 48h of exposure to vapors generated from 500μL of 5% ethanol in light grown root and 8h of exposure to vapors from 500μL of 8% ethanol for dark grown hypocotyl (except particular induction time annotated in the figure legend). In each single experiment, WT and ABP1 conditional lines were always grown on the same plate and exposed to ethanol in identical conditions. *ric1-1* and *rop6-1* were in the *Wassilewskji* (WS) background[16], the other lines were derived from the *Columbia* (Col-0) background. T-DNA insertion mutant of *KTN1* (SAIL_343_D12) was provided from the *Arabidopsis* Information Resource. Offspring of the double mutants were analyzed by PCR amplification as described previously[17, 25]. For the generation of inducible overexpressing ABP1 lines (XVE>>ABP1-OE), ABP1-GFP was cloned by inserting GFP into ABP1 after the glycine 120 by primer extension PCR with two glycines flanking the GFP coding sequence[17], then the fragment of full-length ABP1 genomic DNA with GFP was cloned into the Gateway vector **pMDC7B** using Gateway® cloning technology (www.invitrogen.com). At least three independent lines were used for the analysis (Rakusová et al., unpublished data). MAP4-GFP[8], TUA6-RFP[9] and EB1b-GFP[13] were used as MT markers, and DII::Venus was used as an early auxin response sensor[14].

Confocal microscopy observation

For observations of MTs orientation in root, cells in the transition zone of the primary root were visualized by a vertical Zeiss LSM700 (with 63× objective using hair gel as immersion medium). For observations in dark grown hypocotyl, cells in the elongation zone were visualized by a Nipkow Spinning Disk confocal system (Yokogawa CXU-X1-A1) mounted on Nikon Eclipse Ti E inverted microscope (with 40× oil immersion objective). For dark grown hypocotyls, all manipulations were performed under green light to avoid any light effects on MTs reorientation prior confocal imaging. For all the visualization of auxin-treated seedlings, 1 min manipulation time was needed for applying auxin before imaging. The videos of EB1b trajectory were performed by spinning disc confocal with 63×water immersion objective. Videos were acquired with 300ms exposure time every 500ms by 10min. The settings of excitation and detection were: for GFP: 488nm, 505-550nm; for Venus: 514nm, 527nm; for RFP: 587nm, 610nm. All the images in a single experiment were captured with the same setting. In experiments where rapid MT reorientation was imaged,

the seedlings were gently placed in chamber slides, covered by 0.8% agar contained 1/2MS or liquid 1/2 MS glass slides, and placed on vertical Zeiss 700 along their original direction of growth. When gravistimulation started, slides were rotated with a rotatable stage by 90°, and epidermal cells at the upper and lower layers were individually visualized. For live imaging on DII-Venus, immediately after the beginning of reorientation, the seedlings were scanned every 10min till 1h to follow the evolution of the DII-Venus signal. Additionally, time-lapse visualization was performed as the time indicated (’=minute, ”=second) in figures and all the experiments were repeated at least three times.

Chemical Treatment

NAA (Sigma), IAA (lab 3) and PEO-IAA[21] were dissolved in dimethyl sulfoxide (DMSO), IAA (Sigma, lab 1, 2) and 17-β-estradiol (Sigma) were dissolved in ethanol, and cordycepin (Sigma) was dissolved in ddH_2O. For estradiol induction, three-day-old seedlings were transferred to 2μM 17-β-estradiol containing 1/2 MS solid medium and were grown vertically for 12h or 48h prior observation or protein/RNA extraction. Non-induced XVE>>ABP1-OE was used as a control. For the experiments with short term chemical treatments, four-day-old seedlings were gently placed on chemical-containing plates according to their original direction of growth. For combined treatments with PEO-IAA or cordycepin and 1μM IAA, four-day-old seedlings grown vertically on 1/2MS were first transferred to plates containing 10μM PEO-IAA or 400μM cordycepin for 30min pretreatment (vertically grown), then transferred on the same medium plus 1μM IAA. For the treatment with different concentrations of $CaCl_2$, 1/2MS with vitamins but without $CaCl_2$ was used in comparison with the same medium added of 1 or 10mM $CaCl_2$ or with a standard 1/2MS (1.5mM $CaCl_2$). For short term treatments, seedlings were mounted on 0.8% agar 1/2MS chamber slides or liquid 1/2MS glass slides containing the indicated concentration of auxin, then were immediately imaged.

Gravitropic response

Four-day-old vertically grown seedlings, under light conditions, were reoriented by 90°, and the angles deviating from the original vertical growing direction of primary roots (defined as 0°) were tracked every 30min till 8h.

Quantification Methods

i. For the quantification of the percentage of different cell types, the number of cells at a certain MT orientation type was calculated as a percentage of total measured cells in each root, and different cell types were divided into transversal, oblique, random and longitudinal groups based on prevalent MT arrangement (Fig. 1a). At least 15 different roots were analyzed and at least 8 cells were quantified in each root. For hypocotyl, cells were classified into a MT orientation group depending on the overall angles of MTs for each cell (0-22.5°/157.5-180° for longitudinal, 22.5-67.5°/112.5-157.5° for oblique and 67.5-112.5° for transversal). Angles of MTs were determined both manually and using the plug-in of ImageJ FibrilTool[28]. At least 10 different hypocotyls were analyzed and 100 hypocotyl cells were quantified.

ii. For the quantification of MTs oriented angles in root cells, the number of MTs at a certain angle range was calculated as a percentage of total MTs measured. The longitudinal direction parallel to and going along with the growth axis was defined as 0°, the transversal direction perpendicular to the growth axis was defined as 90°, the longitudinal direction parallel to but going opposite to the growth axis was defined as 180°, and angles deviating from the longitudinal direction (0°) were measured. Different microtubules angles were divided into two categories: transversal direction (90±30°), oblique and longitudinal direction (0-60°/120-180°). The measurement of deviated angles of MTs was processed by ImageJ combined with Matlab inc. At least 8 cells of different roots were randomly selected, and in each cell at least 100 microtubules were quantified.

iii. For the 'time-stack' images of EB1b trajectory (Fig. 1c), the video of EB1b trajectory was taken every 15sec per picture in Zeiss LSM700 for 10min in total, every 3sec per picture in spinning disc for 10min in total. The maximum intensity projections of all frames were stacked by Image J (Image>Stack>Z-project). Then, EB1b trajectory was quantified as described previously (method ii).

iv. For the quantification of the rate of EB1b movement, the method was previously described in details[29]. In brief, the manual quantification of EB1b trajectory (Fig. 3a, b) was performed according to the directions of each single EB1b tracks followed with strips. As we defined before, the longitudinal direction parallel to and going along with the growth axis was defined as 0°, the transversal direction perpendicular to the growth axis was defined as 90°. Blue strips represent transversal direction (90±30°), and red strips represent oblique and longitudinal direction (0-60°/120-180°). The deviated angle of each EB1b strip from transversal direction was measured by ImageJ. At least 10 cells of different roots were randomly selected, and in each cell at least 100 EB1b tracks were quantified.

v. Additionally, automated quantification of the directionality of EB1b trajectory was performed as following steps. To determine the direction of EB1b trajectory within the cells, it is necessary to eliminate the apparent motion caused by the growth of the seedling. In a first step image stabilization was therefore performed by manually locating a prominent feature e.g. the boundary between two specific cells in all frames of the video. Translating each frame accordingly then kept the prominent feature stationary. This proved more accurate than various automated image registration methods.

The temporal resolution of the videos was generally not sufficient to track individual particles over multiple frames. Thus particle tracking velocimetry resulted in a very sparse vector field. In order to obtain a more complete vector field that better represents the transport direction of all reporter proteins, the Horn-Schunck method of estimating optical flow was implemented and subsequently used for the analysis. In this method a regularization parameter enforces a smooth vector field which then assigns a vector of motion (speed and direction) to each pixel and frame of the video filling in the missing flow information from the motion of the neighboring pixels. The regularization parameter was adjusted to

match the visual assessment of the flow. The resulting vector field was afterwards averaged over several frames.

The dominant direction of motion at each pixel was calculated only if the speed reaches a certain threshold which was determined by comparison with the maximum intensity projection of the video where regions with no or little protein transport appear darker. The values chosen for the regularization parameter and the minimum speed were kept constant throughout the analysis of all videos.

The direction of motion of the remaining pixels, for which the speed was above the threshold value, was sorted into two classes: Blue indicates a direction of transport of 90° ±30° and red corresponds to 0°-60°/120°-180°. Finally, the areal fraction of the two classes was calculated.

vi. For the quantification of the fluorescence, DII-Venus fluorescence was pseudo-colored, and the epidermal and cortical cells of similar developmental stages with the symmetric areas in roots were selected for quantification. The intensity of nuclei was extracted using the ROI tool of Fiji software (http://fiji.sc/wiki/index.php/Fiji), and the sum of fluorescence in the upper side and lower side cells of each seedling was individually quantified[14].

qRT-PCR

Whole RNA of seedlings was extracted using the RNeasy Mini Kit (Qiagen) and cDNA was synthesized using iScript cDNA Synthesis Kit (Bio-rad). qRT-PCR analysis was performed using LightCycler® 480 SYBR Green I Master (Roche) following recommendations of the manufacturer. qRT-PCR was carried out in 384-well optical reaction plates by using Perkin Elmer Janus Robot and Roche Lightcycler 480 with heated for 10min to 95°C to activate hot-start *Taq* DNA polymerase, followed by 40 cycles of denaturation for 60s at 95°C and annealing-extension for 60s at 58°C. Expression levels were normalized to the expression levels of *ACTIN8*. Specific primers of *ABP1* (F: TCGTCGTCTTTTCCGTCGCG; R: TTGGCAAGCCATTGATGGGACA) and *ScFv* (F: TTACTGGATGCACTGGGTGA; R: AAGACTGACAGGCAGGGAGA) were used for gene expression as previously reported[19,20]. Two biological repeats were analyzed in triplicates. qRT-PCR relative quantification was performed on the Lightcycler 480 software combined with the local website (http://qpcr.ista.local).

Protein Analysis

Proteins were extracted from WT and XVE>>ABP1-OE ten-day-old seedlings induced or not with estradiol by grinding at 4°C with a mortar in the extraction buffer (50 mM Tris-HCl, pH 7.5, 1 mM EDTA, 100 μM $MgCl_2$, 5 mM sodium ascorbate, 500 mM sucrose, phosphatase and protease inhibitors). Samples were spun at 5000g for 10 min at 4°C to remove cell debris. Supernatants were centrifuged at 50000g for 60 min at 4°C to pellet the total membrane fraction. Pellets were resuspended in microsomal buffer (25 mM Tris-HCl pH 6.8, 0.5 mM EDTA, 0.1 mM $MgCl_2$, 330 mM sucrose, 10% glycerol, protease inhibitor cocktail) for the following SDS-PAGE analysis. Protein loading was controlled by coomassie brilliant blue staining. Protein gel blot analysis was performed by using the

mAb12 mouse monoclonal antibody[30] to detect ABP1 protein. Protein amount was specified by GelQuant. NET software and normalized according to sample loading. Two biological repeats were analyzed in duplicates.

Statistics

For all quantitative data, error bars indicate standard error mean (s.e.m.). The number of analyzed samples is indicated as n from at least three biological replicates, and statistical analyses were performed using student's T-test where * or ** corresponds to p-value <0.05 or 0.001, respectively.

Extended Data

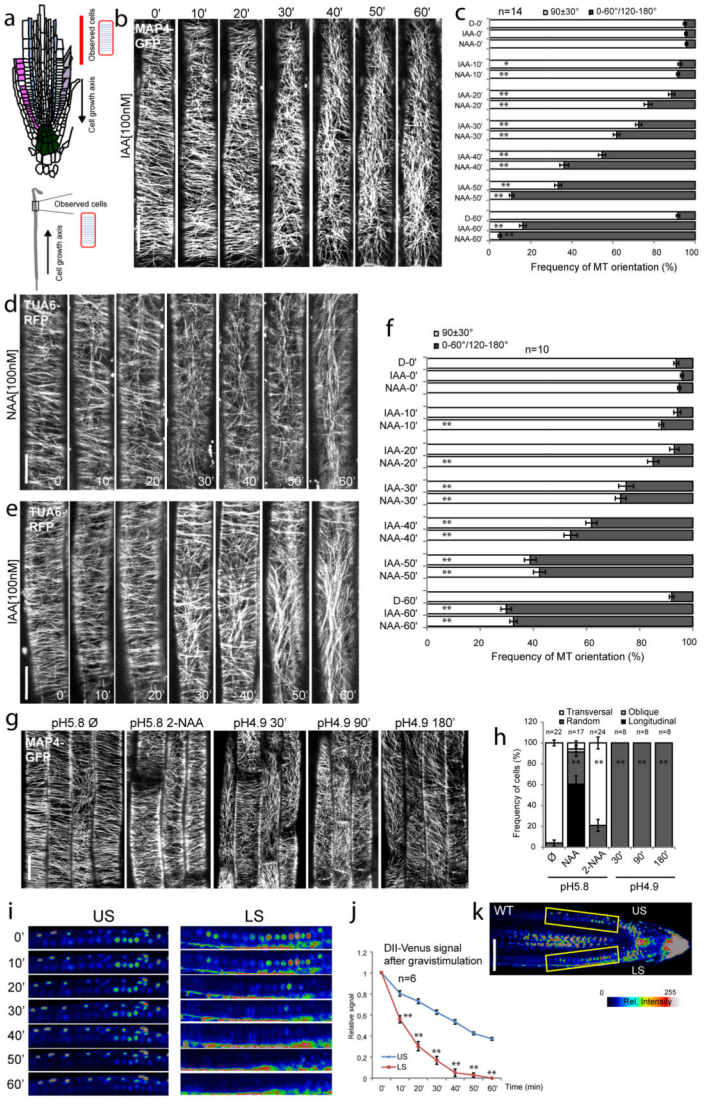

Extended Data Figure 1. Auxin induces MT rearrangement in root cells

Europe PMC Funders Author Manuscripts

Europe PMC Funders Author Manuscripts

(a) Schematic diagram of root and dark grown hypocotyl growth. The growth direction of root and hypocotyl is named as cell growth axis. The observed cells for MTs array were in the transition zone (highlighted by red line) of root and in the elongation zone of dark grown hypocotyl (highlighted by grey frame). The arrays of MTs in root and hypocotyl were depicted for the expanding cells.

(b-f) MAP4-GFP or TUA6-RFP visualization of MTs orientation in roots was performed by time-lapse observation (every 10min, '=min) following 100nM NAA or IAA treatment, and deviated angles of individual MTs were quantified as transversal MTs (90±30°) or longitudinal MTs (0-60°/120-180°). In (c) and (f), Student's T-test was calculated for transversal MTs in comparison to untreated roots (* $p<0.05$; ** $p<0.001$).

(g-h) MAP4-GFP visualization and quantification of MTs orientation in roots after 1μM 2-NAA treatment for 60min or after transfer of seedlings on acidified 1/2 MS medium at pH4.9 for 30min, 90min and 180min. Student's T-test was calculated for transversal MTs in treated samples in comparison to 1/2MS (pH5.8) growing roots used as controls (** $p<0.001$).

(i-k) Auxin distribution approximated by DII-Venus at the lower side (LS) and upper side (US) of 90° reoriented WT root (in DII-Venus background). Enlarged pictures (i) are shown as the frames highlighted (k). Signal intensity is represented by the color code as indicated. The relative signal for the US and LS (j) is expressed in comparison to the signal in the respective frame before gravistimulation. Student's T-test was calculated for the signal between US and LS at each time point (** $p<0.001$).

In all panels, error bars are s.e.m. Scale bars: 5 μm (b, d, e, g) and 30 μm (k).

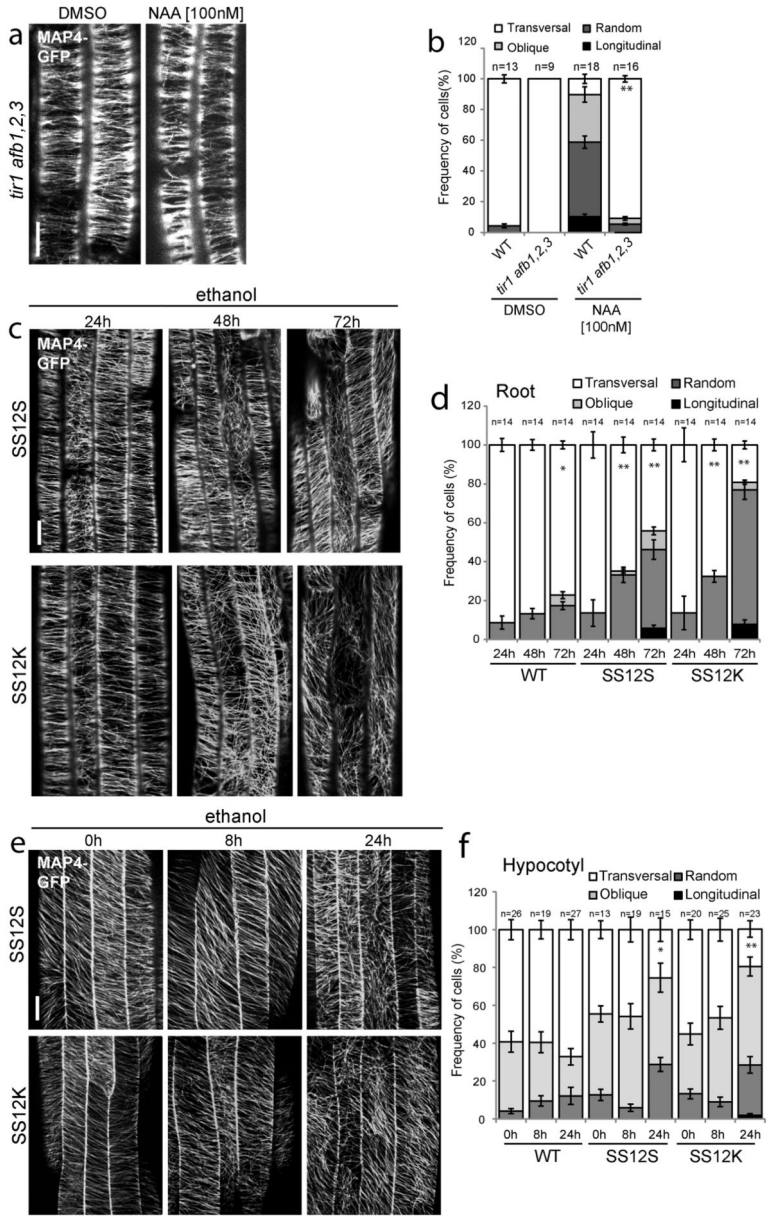

Extended Data Figure 2. Functional inactivation of ABP1 resulted in MT defects gradually increasing with time of ABP1 inactivation

(a-b) MAP4-GFP visualization of MTs orientation in WT and *tir1-1afb1-1afb2-1afb3-1* (abbreviated as *tir1afb1,2,3)* seedlings following 100nM NAA treatment for 60min. The proportion of cells with the four categories of MTs orientation patterns was determined, and the student's T-test was calculated for the category of transversal MT in comparison to WT treated in the same condition (** $p<0.001$).

(c-f) MAP4-GFP visualization and quantification of MTs orientation in roots (c-d) or dark grown hypocotyls (e-f) of WT, SS12S and SS12K seedlings following different time of

Europe PMC Funders Author Manuscripts

ethanol induction as indicated. Student's T-test was calculated for the transversal MTs in comparison to WT exposed for the same time to ethanol vapors than the conditional ABP1 lines (* $p<0.05$, ** $p<0.001$).

In all panels, error bars are s.e.m. Scale bars: 5μm (a, c) and 10μm (e).

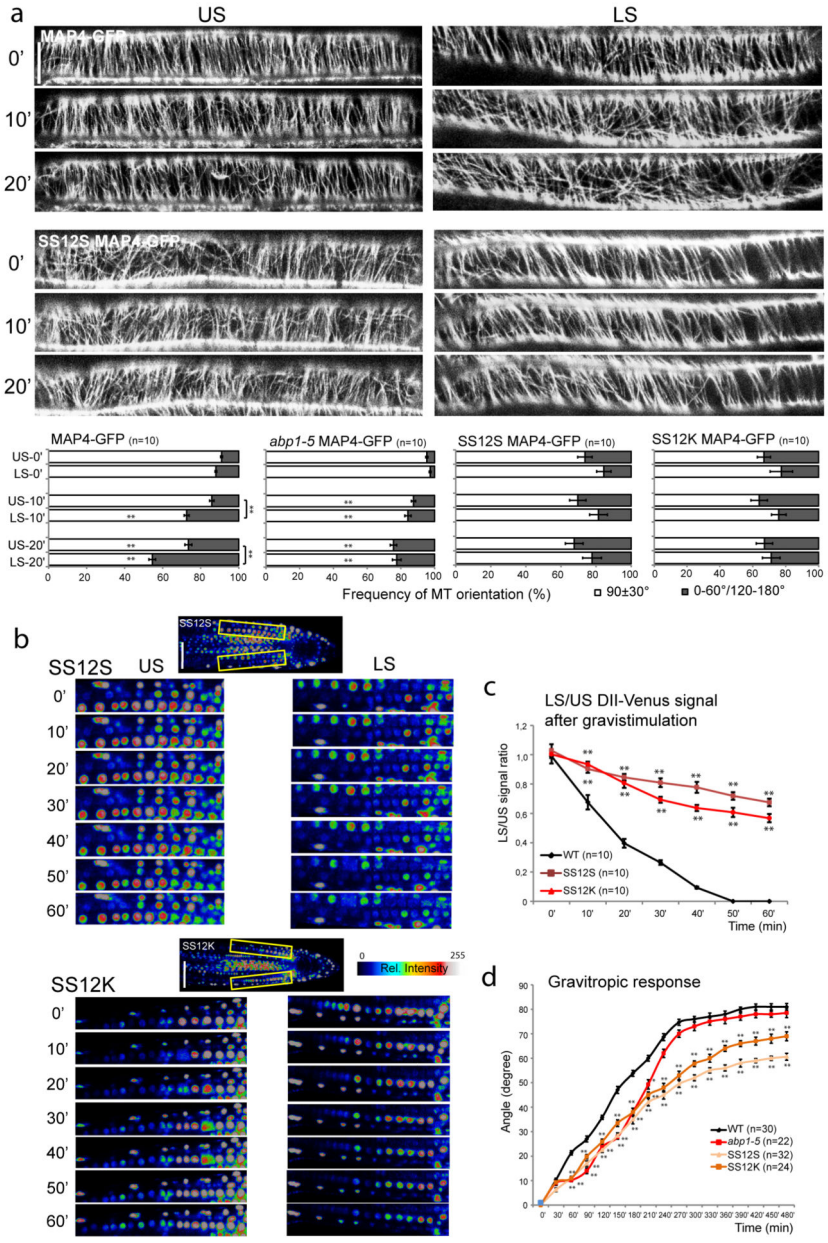

Extended Data Figure 3. ABP1 is involved in MT rearrangement following gravistimulation

(a) Rearrangement of MTs at the LS compared with the US of 90° reoriented roots of WT, SS12S, SS12K, *abp1-5* (all expressing MAP4-GFP). Two different types of MTs orientation (90±30° or 0-60°/120-180°) were quantified. Student's T-test was calculated for the

Europe PMC Funders Author Manuscripts

category of transversal MTs in comparison to each 0' time point and calculated for transversal MTs in the LS in comparison of the US at each time point (** $p<0.001$).
(b-c) Auxin distribution simulated by DII-Venus at the LS compared with the US of 90° reoriented roots of SS12S and SS12K (all in DII-Venus background, enlarged pictures was visualized as the frames highlighted). Image stacks were taken every 10min, and in total 60 min ('). The ratio of the LS signal divided by the US one is shown in the chart (c). Student's T-test was calculated for the signal ratio at each time point of SS12S/K compared with WT (** $p<0.001$). Signal intensity is represented by the color code as indicated. To be compared to WT data (Extended Data Fig. 1i-k).
(d) The deviated angles of 90° gravistimulated-roots of WT, *abp1-5*, SS12S and SS12K seedlings were calculated for every 30min, in total 8h (Student's T-test, *$p<0.05$, ** $p<0.001$).
In all panels, error bars are s.e.m. Scale bars: 5 μm (a) and 30 μm (b).

Europe PMC Funders Author Manuscripts

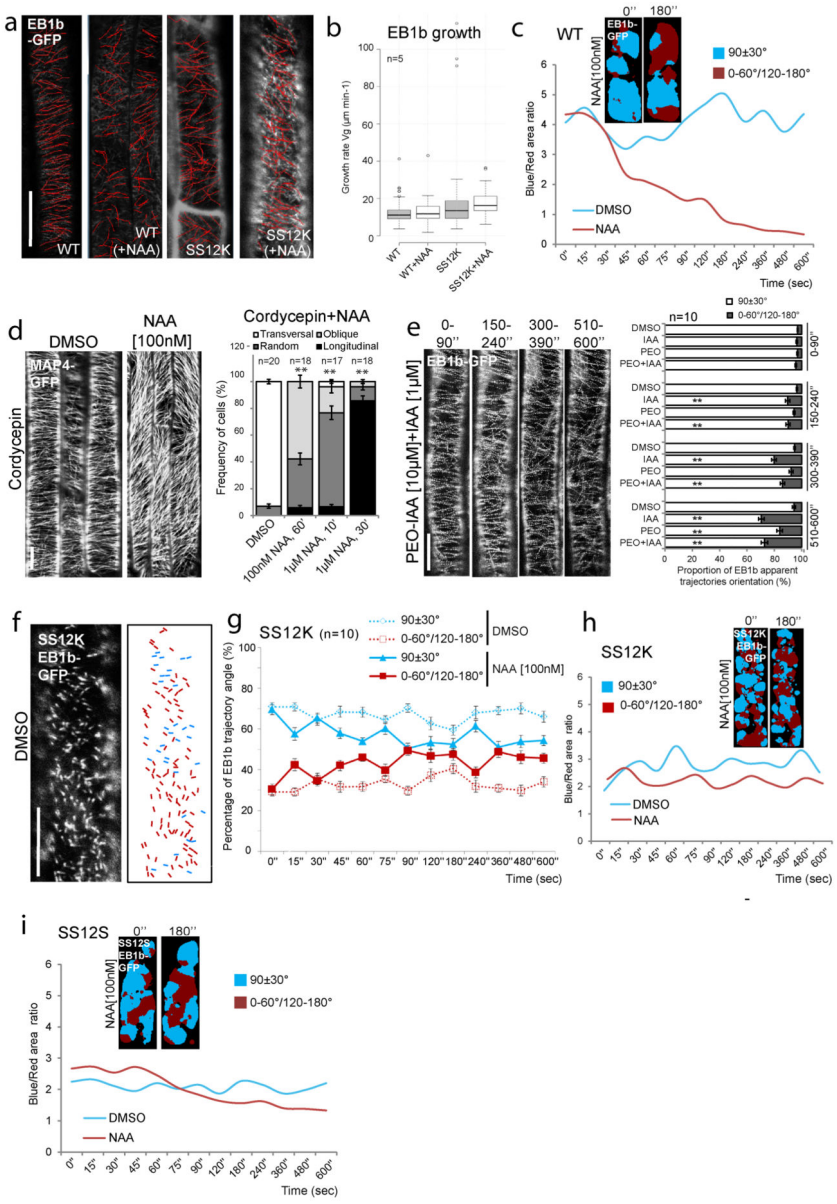

Extended Data Figure 4. Auxin effect on fast responsiveness of MT dynamics is dependent on ABP1

(a-b) Acquisition and quantification of the rate of EB1b movement in roots of untreated or 100nM NAA-treated (60min) WT or SS12K (expressing EB1b-GFP) by measuring EB1b-GFP growth events as highlighted by red lines (Student's T-test, $p>0.05$). Box plots indicate the 25 percentage (bottom boundary), median (middle line), 75 percentage (top boundary), the nearest observations within 1.5 times, the interquartile range and outliers.

(c) EB1b movement was simulated as transversal (blue, 90±30°) or longitudinal (red, 0-60°/120-180°) trajectories before (0") and after 180"100 nM NAA treatment in WT background

(color maps). The blue/red surface ratio is quantified as the chart (n=5). Corresponding to Fig. 3a.

(d) MTs orientation patterns after 400μM cordycepin plus NAA cotreatment. Student's T-test was calculated for the category of transversal MT in comparison to only cordycepin treatment (** $p<0.001$).

(e) EB1b trajectories (simulated by time-stack from 10min videos) were visualized and quantified after DMSO, IAA (1μM), PEO-IAA (10μM), and PEO-IAA (10μM) plus IAA (1μM) treatments. The left panel shows successive frames of 90sec acquisitions following IAA application of pretreated PEO-IAA WT roots. Student's T-test was calculated for the category of transversal MTs in comparison to DMSO treatment at each time point (** $p<0.001$).

(f-i) Projections of EB1b-GFP in SS12K roots (f) and quantification (g) from every 15 sec acquisitions during 10 min (Supplementary Video 4, 6) following DMSO or 100 nM NAA application (n=10). Blue and red strips represent transversal (90±30°) and oblique/longitudinal (0-60°/120-180°) directions, respectively (f). Color maps show the simulated transversal or longitudinal trajectories of EB1b before (0") and after 180"100 nM NAA treatment in SS12K (h) or SS12S (i) roots. The blue/red surface ratio is quantified as the charts (n=5) (h-i). The data of SS12S (i) is corresponding to Fig. 3b. Compared to WT situation (Fig. 3a, Extended Data Fig. 4c).

In all panels, error bars are s.e.m and scale bars are 5 μm.

Europe PMC Funders Author Manuscripts

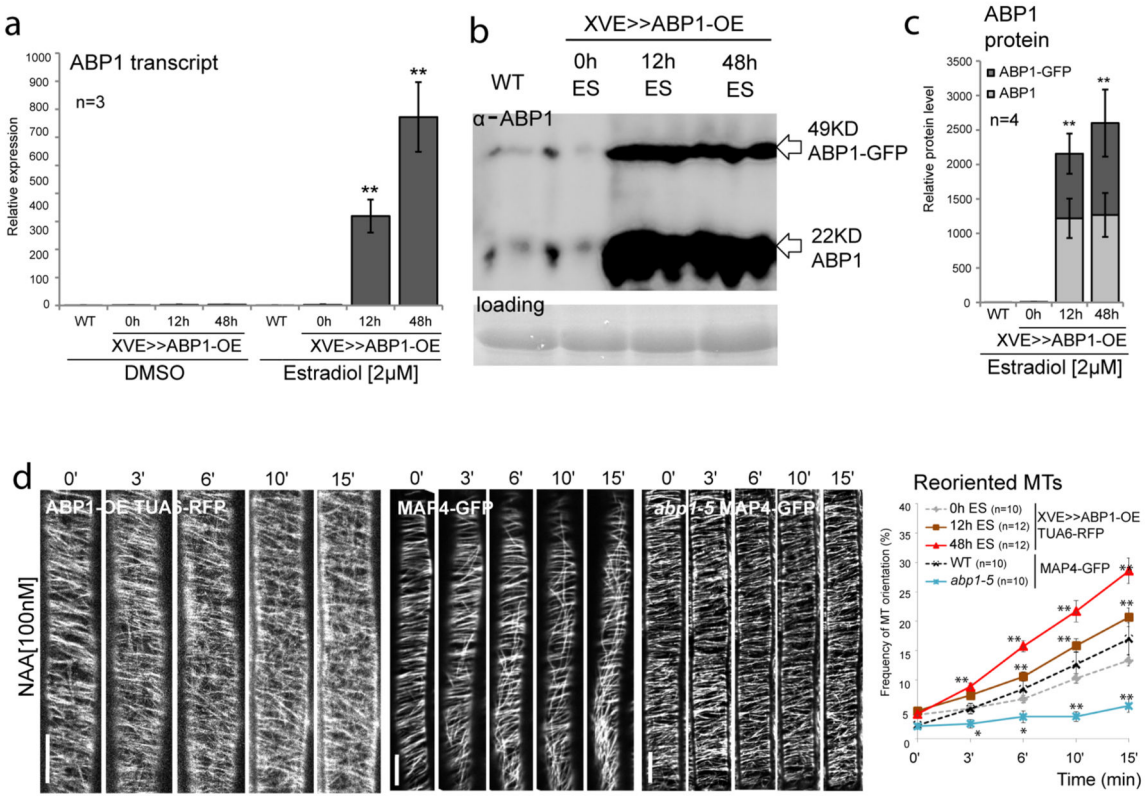

Extended Data Figure 5. Overexpressed ABP1 induced auxin effect on fast responsiveness of MT dynamics

(a-c) ABP1 and ABP1-GFP transcripts (a) and ABP1 protein level (b-c) were detected in WT and XVE>>ABP1-OE line before and after 2μM estradiol induction for 12h or 48h prior to RNA or protein extraction. The transcript levels of ABP1 in WT with DMSO treatment was standardized as "1" (a). 22KDa native ABP1 band and 49KDa ABP1-GFP band were detected and quantified in the right chart. The protein level of native ABP1 or ABP1-GFP in WT was standardized as "1" for each ABP1 and ABP1-GFP, respectively (b-c). Student's T-test, ** $p<0.001$.

(d) Time-lapse observation of MTs orientation in the roots of XVE>>ABP1-OE roots expressing TUA6-RFP, WT and *abp1-5* (both expressing MAP4-GFP) upon 100 nM NAA treatment. The percentage of reorientated MTs (0-60°/120-180°) was quantified. Reorientated MTs in the inducible XVE>>ABP1-OE TUA6-RFP roots were calculated in comparison to none-inducible roots, and *abp1-5* MAP4-GFP was compared to MAP4-GFP situation at each time point (Student's T-test, * $p<0.05$, ** $p<0.001$).

In all panels, error bars are s.e.m and scale bars are 5 μm.

Europe PMC Funders Author Manuscripts

Europe PMC Funders Author Manuscripts

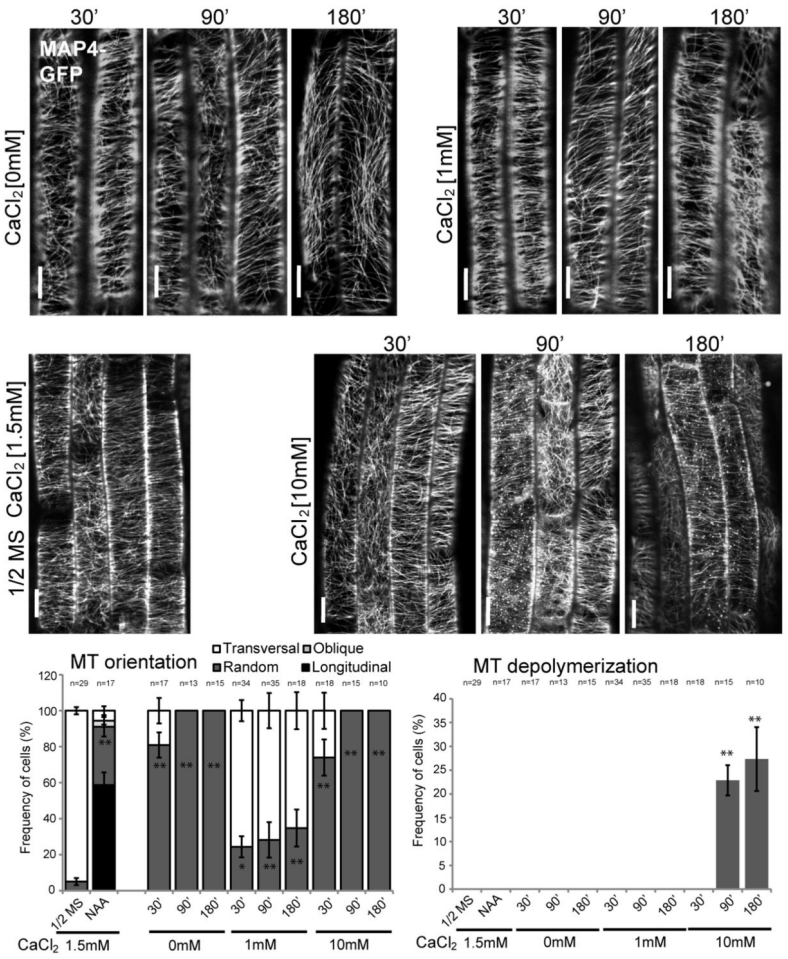

Extended Data Figure 6. Calcium starvation disrupts MT orientation and high calcium increases MT depolymerization

Orientation and polymerization status of MTs were visualized following transfer of seedlings to different concentrations of $CaCl_2$ for 30min, 90min or 180min. Low calcium level disrupted MTs organization leading to predominantly random pattern and high calcium caused MT depolymerization. Student's T-test was calculated for the category of transversal MTs in comparison to seedlings grown and transferred on standard 1/2 MS (with 1.5mM $CaCl_2$) seedlings (*$p<0.05$, ** $p<0.001$). In all panels, error bars are s.e.m. and scale bars are 5μm.

Europe PMC Funders Author Manuscripts

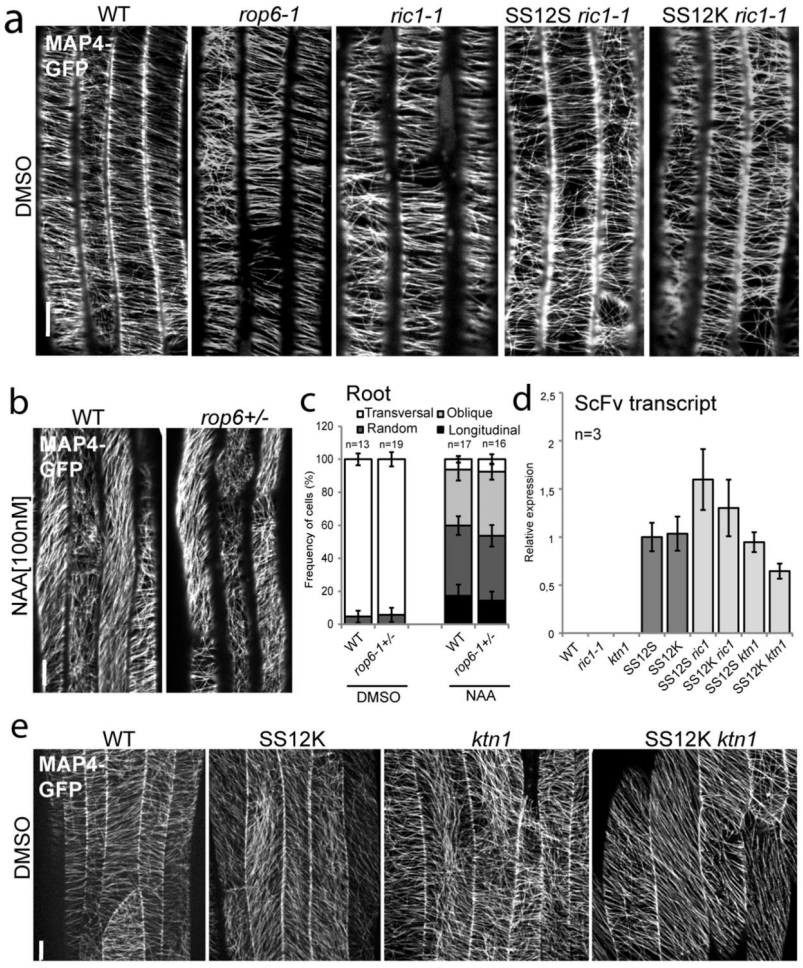

Extended Data Figure 7. Auxin-ABP1 controls MT arrangement through the downstream ROP6-RIC1-KTN1 signaling

(a) MAP4-GFP visualization of MTs orientation in the root of WT, *rop6-1*, *ric1-1*, SS12S *ric1-1*, SS12K *ric1-1* following DMSO application for 60 min. Corresponding to quantifications in Fig. 4a.

(b-c) MTs reorientation patterns were visualized by MAP4-GFP in the roots of WT and *rop6-1*$^{+/-}$ following DMSO or 100nM NAA application for 60 min (Student's T-test, $p>0.05$).

(d) The transcript level of the *scFv12* coding the recombinant antibody responsible for ABP1 knockdown in WT, *ric1-1*, *ktn1*, SS12S, SS12K, SS12S *ric1-1*, SS12K *ric1-1*, SS12S *ktn1* and SS12K *ktn1* after 48h ethanol induction. The transcript level of the *scFv12* in SS12S was standardized as "1" (Student's T-test, $p>0.05$).

(e) MTs orientation by MAP4-GFP in dark grown hypocotyls of WT, SS12K, *ktn1*, SS12K *ktn1* (with 24h ethanol induction) following DMSO application for 60 min. Corresponding to Fig. 4b. In all panels, error bars are s.e.m. Scale bars: 5μm (a-b) and 10μm (d).

Supplementary Material

Refer to Web version on PubMed Central for supplementary material.

Acknowledgements

We thank Ram Dixit for carrying out complementary experiments, David W Ehrhardt and Takashi Hashimoto for providing the seeds of TUB6-RFP and EB1b-GFP, respectively; Eva Zazimalova, Jan Petrasek and Matyas Fendrych for helpful discussion of the manuscript and Jeff Leung for efficient text optimization. This work was supported by the European Research Council (project ERC-2011-StG-20101109-PSDP) to J.F., ANR blanc AuxiWall project ANR-11-BSV5-0007 (C.P-R and L.G.) and the Agency for Innovation by Science and Technology (IWT) to H.R.. This work has benefited from the facilities and expertise of the Imagif Cell Biology platform (www.imagif.cnrs.fr) which is supported by the Conseil Général de l'Essonne.

References

1. Perrot-Rechenmann C. Cellular responses to auxin: division versus expansion. Cold Spring Harb. Perspect. Biol. 2010; 2:a001446. [PubMed: 20452959]
2. Sedbrook JC, Kaloriti D. Microtubules, MAPs and plant directional cell expansion. Trends Plant Sci. 2008; 13:303–310. [PubMed: 18467155]
3. Chapman EJ, Estelle M. Mechanism of auxin-regulated gene expression in plants. Annu. Rev. Genet. 2009; 43:265–285. [PubMed: 19686081]
4. Lucas J, Shaw SL. Cortical microtubule arrays in the Arabidopsis seedling. Curr. Opin. Plant Biol. 2008; 11:94–98. [PubMed: 18226578]
5. Blancaflor EB. The cytoskeleton and gravitropism in higher plants. J. Plant Growth Regul. 2002; 21:120–136. [PubMed: 12024227]
6. Lindeboom JJ, et al. A mechanism for reorientation of cortical microtubule arrays driven by microtubule severing. Science. 2013; 342:1245533. [PubMed: 24200811]
7. Ubeda-Tomas S, Beemster GT, Bennett MJ. Hormonal regulation of root growth: integrating local activities into global behaviour. Trends Plant Sci. 2012; 17:326–331. [PubMed: 22401844]
8. Marc J, et al. A GFP-MAP4 reporter gene for visualizing cortical microtubule rearrangements in living epidermal cells. Plant Cell. 1998; 10:1927–1940. [PubMed: 9811799]
9. Chan J, Calder G, Fox S, Lloyd C. Cortical microtubule arrays undergo rotary movements in Arabidopsis hypocotyl epidermal cells. Nat. Cell Biol. 2007; 9:171–175. [PubMed: 17220881]
10. Collett CE, Harberd NP, Leyser O. Hormonal interactions in the control of Arabidopsis hypocotyl elongation. Plant Physiol. 2000; 124:553–562. [PubMed: 11027706]
11. Simon S, et al. Defining the selectivity of processes along the auxin response chain: a study using auxin analogues. New Phytol. 2013; 200:1034–1048. [PubMed: 23914741]
12. Morita MT. Directional gravity sensing in gravitropism. Annu. Rev. Plant Biol. 2010; 61:705–720. [PubMed: 19152486]
13. Chan J, Calder GM, Doonan JH, Lloyd CW. EB1 reveals mobile microtubule nucleation sites in Arabidopsis. Nat. Cell Biol. 2003; 5:967–971. [PubMed: 14557818]
14. Brunoud G, et al. A novel sensor to map auxin response and distribution at high spatio-temporal resolution. Nature. 2012; 482:103–106. [PubMed: 22246322]
15. Tromas A, et al. Auxin-Binding Protein 1 is a negative regulator of the SCF(TIR1/AFB) pathway. Nat. Commun. 2013; 4:2496. [PubMed: 24051655]
16. Xu T, et al. Cell surface- and rho GTPase-based auxin signaling controls cellular interdigitation in Arabidopsis. Cell. 2010; 143:99–110. [PubMed: 20887895]

17. Robert S, et al. ABP1 mediates auxin inhibition of clathrin-dependent endocytosis in Arabidopsis. Cell. 2010; 143:111–121. [PubMed: 20887896]
18. Dharmasiri N, et al. Plant development is regulated by a family of auxin receptor F box proteins. Dev. Cell. 2005; 9:109–119. [PubMed: 15992545]
19. Braun N, et al. Conditional repression of AUXIN BINDING PROTEIN1 reveals that it coordinates cell division and cell expansion during postembryonic shoot development in Arabidopsis and tobacco. Plant Cell. 2008; 20:2746–2762. [PubMed: 18952781]
20. Tromas A, et al. The AUXIN BINDING PROTEIN 1 is required for differential auxin responses mediating root growth. PLoS One. 2009; 4:e6648. [PubMed: 19777056]
21. Hayashi K, et al. Small-molecule agonists and antagonists of F-box protein-substrate interactions in auxin perception and signaling. Proc. Natl. Acad. Sci. U S A. 2008; 105:5632–5637. [PubMed: 18391211]
22. Shishova M, Lindberg S. A new perspective on auxin perception. J. Plant Physiol. 2010; 167:417–422. [PubMed: 20176409]
23. Uyttewaal M, et al. Mechanical stress acts via katanin to amplify differences in growth rate between adjacent cells in Arabidopsis. Cell. 2012; 149:439–451. [PubMed: 22500806]
24. Lin D, et al. Rho GTPase signaling activates microtubule severing to promote microtubule ordering in Arabidopsis. Curr. Biol. 2013; 23:290–297. [PubMed: 23394835]
25. Chen X, et al. ABP1 and ROP6 GTPase signaling regulate clathrin-mediated endocytosis in Arabidopsis roots. Curr. Biol. 2012; 22:1326–1332. [PubMed: 22683261]
26. Paciorek T, et al. Auxin inhibits endocytosis and promotes its own efflux from cells. Nature. 2005; 435:1251–1256. [PubMed: 15988527]
27. Montagnac G, et al. alphaTAT1 catalyses microtubule acetylation at clathrin-coated pits. Nature. 2013; 502:567–570. [PubMed: 24097348]
28. Boudaoud A, et al. FibrilTool, an ImageJ plug-in to quantify fibrillar structures in raw microscopy images. Nature protocols. 2014; 9:457–463. [PubMed: 24481272]
29. Salaycik KJ, Fagerstrom CJ, Murthy K, Tulu US, Wadsworth P. Quantification of microtubule nucleation, growth and dynamics in wound-edge cells. J. Cell Sci. 2005; 118:4113–4122. [PubMed: 16118246]
30. Leblanc N, et al. A novel immunological approach establishes that the auxin-binding protein, Nt-abp1, is an element involved in auxin signaling at the plasma membrane. J. Biol .Chem. 1999; 274:28314–28320. [PubMed: 10497189]

Europe PMC Funders Author Manuscripts

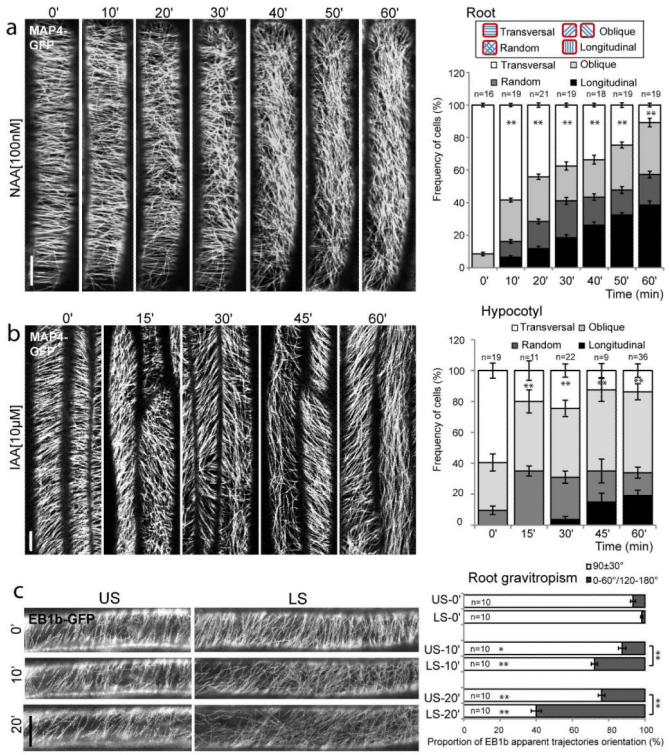

Figure 1. Auxin induces MT reorientation

(a-b) MAP4-GFP visualization of MTs orientation in roots (a) and etiolated hypocotyls (b) by time-lapse imaging following 100 nM NAA or 10 µM IAA treatment, respectively. The cartoon illustrates the four categories of MTs orientation.

(c) EB1b-GFP visualization of MTs trajectories at the LS and US sides of 90° gravistimulated roots. EB1b trajectories were quantified as transversal (90±30°) or longitudinal (0-60°/120-180°) MTs.

In all panels, error bars are s.e.m. and student's T-test was calculated for transversal MTs (*p<0.05, ** p<0.001). Scale bars: 5 µm (a, c), 10 µm (b).

Europe PMC Funders Author Manuscripts

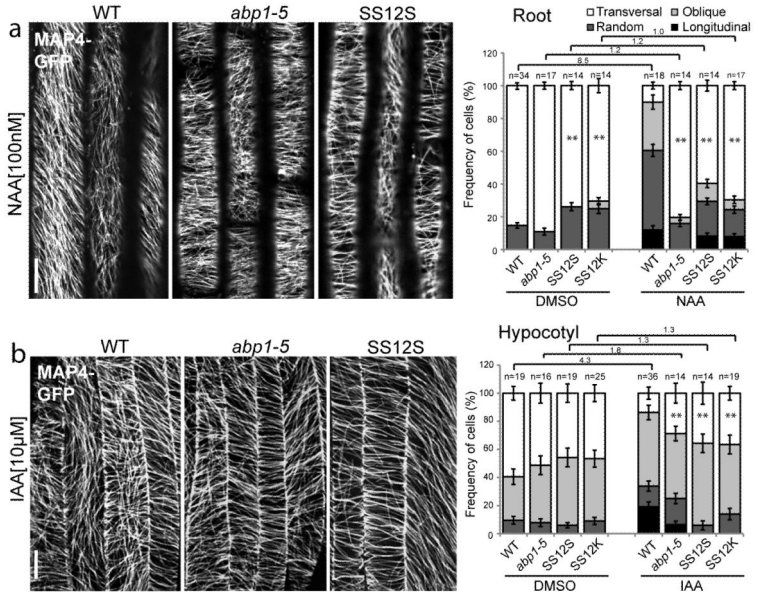

Figure 2. ABP1 is required for auxin regulation of MT reorientation

(a-b) MAP4-GFP visualization of MTs reorientation in WT, *abp1-5*, SS12S/K root (a) and hypocotyl (b) induced with ethanol vapors for 48h (a) and 8h (b) and following 60 min treatment with DMSO, 100 nM NAA (a) or 10 μM IAA (b). The ratio of transversal MTs in DMSO-versus NAA-treated is indicated above the charts (a, b). In all panels, error bars are s.e.m. and student's T-test was calculated for transversal MTs (** $p<0.001$). Scale bars: 5 μm (a) and 10 μm (b).

Europe PMC Funders Author Manuscripts

Europe PMC Funders Author Manuscripts

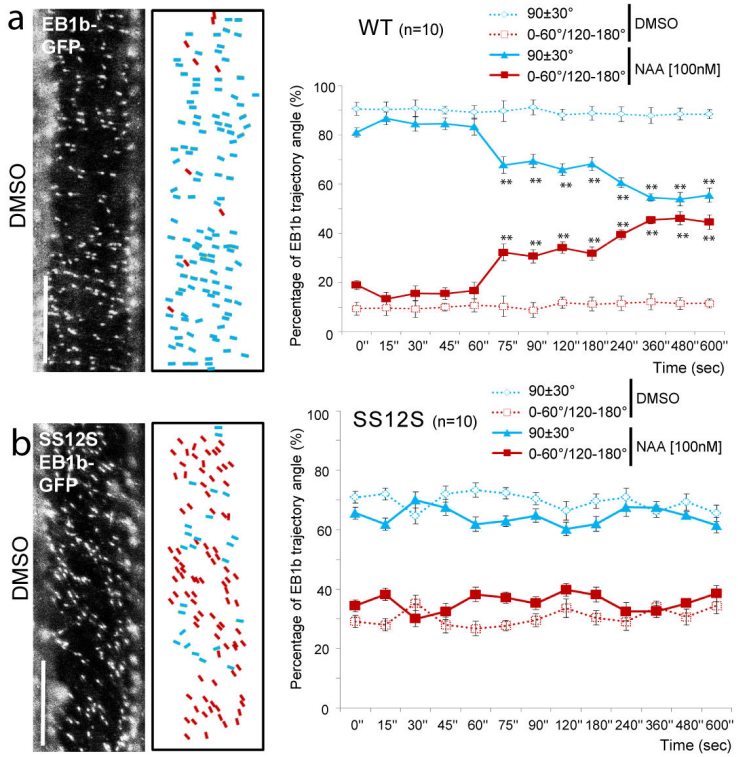

Figure 3. Auxin effect on fast responsiveness of MT rearrangement is dependent on ABP1

(a-b) Projections of EB1b-GFP in WT (a) or SS12S (b) roots (left panels) and quantification (right charts) from every 15 sec acquisitions during 10 min (Supplementary Video 1, 2, 3, 5) following DMSO or 100 nM NAA application (n=10). Blue and red strips represent transversal (90±30°) and oblique/longitudinal (0-60°/120-180°) directions, respectively. In all panels, error bars are s.e.m. determined by student's T-test (*p<0.05, ** p<0.001). Scale bars: 5 μm.

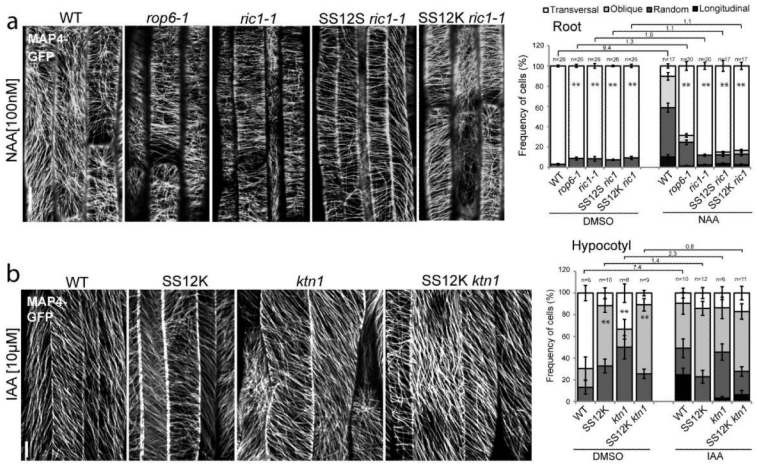

Figure 4. Auxin-ABP1 control MT arrangement through downstream ROP6-RIC1 and involvement of KTN1

(a) MTs orientation and quantification in roots of WT, *rop6-1*, *ric1-1*, SS12S/K *ric1-1* following 60 min of DMSO or 100 nM NAA application.

(b) MTs orientation and quantification in 24h ethanol induced hypocotyls of WT, SS12K, *ktn1* and SS12K *ktn1* following 60 min of DMSO or 10 μM IAA application.

The ratio of transversal MTs in DMSO-versus NAA/IAA-treated is indicated above the charts (a, b). In all panels, error bars are s.e.m. and student's T-test was calculated for transversal MTs (** $p<0.001$). Scale bars: 5 μm (a) and 10 μm (b).

Europe PMC Funders Author Manuscripts